EAI Endorsed Transactions
on Scalable Information Systems
Research Article EAI.EU

Quantum Communication-Assisted Synchronization Framework for Distributed 3D Power Grid Models Across Multi-Regional Control Centers

Youhui Chen[1,*], Zhonghua Lv[1], Ruixue Hu[1], Xinying Zhao and Dongxue Li[1]

[1]State Grid Liaoning Electric Power Company Limited Economic Research Institute, Shenyang 110015, China

Abstract

INTRODUCTION: The synchronization of three-dimensional digital twin models across geographically distributed power grid control centers represents a critical challenge in modern power system operations. Traditional synchronization methods including Network Time Protocol (NTP) and Precision Time Protocol (PTP) achieve only millisecond-level accuracy, which proves fundamentally insufficient for monitoring and responding to critical power grid transients that occur on sub-millisecond timescales. The proliferation of renewable energy sources and distributed generation resources further intensifies synchronization requirements. OBJECTIVES: This research develops a comprehensive quantum communication-assisted synchronization framework designed to achieve unprecedented temporal accuracy for distributed 3D power grid models spanning multi-regional control centers while maintaining compatibility with existing infrastructure. METHODS: A hierarchical quantum-classical hybrid architecture is proposed that strategically utilizes quantum entanglement channels for time-critical synchronization signals and classical communication channels for bulk data transmission. An adaptive fault-tolerance mechanism dynamically adjusts quantum error correction strategies based on real-time quantum channel quality assessments, with graceful degradation to classical protocols when necessary. RESULTS: Extensive simulations utilizing 128 IEEE 118-bus system models demonstrate sub-10 nanosecond synchronization precision—representing 10,000-fold improvement over NTP—with end-to-end latencies maintained below 10 microseconds. The framework exhibits robust performance with synchronization success rates exceeding 90% under 15% node failure conditions and demonstrates logarithmic O(log M) time complexity compared to O(M^2) scaling for classical consensus protocols. CONCLUSION: The quantum communication-assisted framework delivers superior accuracy, scalability, and fault tolerance compared to classical synchronization protocols, establishing viability for next-generation smart grids with extensive distributed energy resources.

Keywords: Quantum communication, Power grid, Digital twin, Quantum entanglement, Distributed energy resources

Received on 15 September 2025, accepted on 18 October 2025, published on 24 February 2026

doi: 10.4108/eetsis.12031

1. Introduction

Complex cyber-physical networks such as the present-day electrical power grids involve widespread geographical areas and are comprised of various types of generation resources such as traditional thermally powered stations, renewable energy resources, energy storage devices, and distributed resources [1]. The successful management and control processes within these large-scale interconnected electrical grids are highly dependent on real-time awareness

*Corresponding author. Email: 7739242@163.com

capabilities that are made possible through the accurate synchronization of digital twin models within various regional control centers [2]. These digital models are virtual representations of the real-world electrical grids that include electrical values such as voltage magnitudes, phase angles, active and reactive power flow values, and dynamic conditions of thousands of components spread over continents [3].

The requirements imposed on digital twin models in the area of synchronized data exchange are further tightening with the development of more complex and dynamically variable power grids. The use of inverter-based renewable energy resources causes sub-second variations of generation activity [4]. Electrically driven charging stations produce rapid variations of the load profile with an impact spreading over the borders of regions [5]. Wide area monitoring grids produce extensive data streams with rates similar to 30 to 120 frames/sec read from phasor measurement units (PMUs) [6]. To ensure stabilized operations and subsequent synchronized reactions to critical phenomena, regional grids are to be updated with synchronized digital models in time intervals below 100-500 ms corresponding to critical processes in electrical grids such as electro-mechanical oscillations and voltage collapses [7].

The present synchronization infrastructure in the power grids is mainly based on traditional communication protocols and techniques. The Network Time Protocol (NTP), commonly adopted among devices connected to the internet, provides synchronization within 1-50 ms with optimal settings [8]. Yet, the accuracy of NTP synchronization deteriorates drastically in heavily loaded networks and over multiple routing layers, with error margins often above 100 ms over continent-wide networks [9]. These margins are clearly undesirable in time-critical applications within the power grid, as the error ranges are about to enter or already exceed the characteristic timescales of transients (100-1000 ms) and sub-synchronous oscillations (10-100 ms) [10].

The Precision Time Protocol (PTP), standardized as IEEE 1588, provides better precision with synchronization accuracy in the microsecond to submicrosecond range [11]. The PTP protocol provides this precision with the aid of hardware timestamping and specialized network infrastructures. But the implementation of PTP faces many challenges in large-scale environments in the power grids. The PTP protocol has to be supported by hardware in network switches and routers on the entire communication path. This results in significant infrastructural costs and compatibility problems within heterogeneous regional networks [12]. Additionally, the PTP protocol experiences deteriorated accuracy with the traversal of non-PTP-aware networks within the entire communication path, making it inappropriate within multi-regional grids with various communication infrastructures [13].

In addition to these protocol constraints, there are fundamental physical limitations that apply to all classical synchronization techniques due to the speed of propagation of electromagnetic signals. The speed limit imposed by the special theory of relativity is 300,000 kilometers/sec; that is, the speed of light in free space [14]. The propagation speed through fiber-optic cables is lower due to the fiber's refractive index and is reported to be about 200,000 kilometers/sec [15]. Assuming transcontinental-scale RMS grids that are 3,000-5,000 kilometers apart, the round-trip time difference due to light speed delays would be 15-25 milliseconds [16]. When the entire delay due to signal routing within the network nodes, protocol overheads, and delays are taken into account, end-to-end delays in excess of 50-100 milliseconds are conceivable [17].

Consensus-based synchronization techniques like those in Paxos, Raft, and Byzantine fault-tolerant algorithms ensure reliable coordination among components in distributed architectures [18]. Yet these approaches come with significant communication overhead, which becomes unscalable with an increase in the number of components. The various traditional consensus approaches are inherently inefficient since they may involve O (N^2) communication overhead among N participating components to attain consensus, thus introducing critical scaling challenges in real-world applications with hundreds and thousands of regional sub-stations in the power grids [19]. The delay with such consensus approaches becomes worse with the increase in the number of components [20].

Recent breakthroughs in the area of quantum information science have made possible the development of practical quantum communication technologies that provide novel functionalities for cooperative behavior in distributed systems [21]. In contrast to quantum computing, which still remains mainly in its research stages, quantum communication has matured to the stage of operational applications in various countries [22].

The Quantum Key Distribution (QKD) protocols BB84 and E91 allow unconditionally secure communication over distances by taking advantage of quantum mechanical principles [23]. Commercial QKD solutions are already installed in metropolitan fiber networks spanning different continents, with more than two dozen quantum-secured communication connections established in the financial, governmental, and telecommunication sectors [24]. The quantum communication backbone network built between Beijing and Shanghai in 2017 spans 2,000 kilometers and connects metropolitan areas with quantum-secured communication lines [25]. The satellite 'Micius', launched in 2016, has already proven intercontinental quantum communication and has successfully established quantum connections over more than 7,600 kilometers between ground stations [26].

Quantum timing and synchronization techniques are another established area within quantum communication. Entanglement-based clock synchronization techniques enable the establishment of time references between distant sites without the need to exchange classical messages in both directions, thus overcoming the latency constraints that hinder classical clock synchronization techniques [27]. Demonstration experiments have shown sub-100 ps clock synchronization with entangled photon pairs over fiber-optic channels [28]. Experiments over satellite links have substantiated the potential use of quantum clock synchronization over continental distances [29].

Quantum communication networks use quantum repeaters to increase the distance coverage of quantum channels beyond 50-100 kilometers due to the limitation caused by the loss of photons in optical fibers [30]. State-of-the-art quantum repeater technology utilizing quantum memories and entanglement swapping has been shown to enable distances above 500 kilometers to be covered over quantum channels [31]. Hybrid quantum-classical networks consisting of quantum communication channels carrying time-critical signals and classical communication channels carrying data offer viable platforms to integrate quantum technologies within current communication settings [32].

Although there has been notable progress in the digitalization of the power grid and the development of quantum communication technology, there has been no research in the area that combines these two areas. The application of quantum to the power sector has been covered in various research works with either quantum computing applications to optimize tasks such as unit commitment and optimal power flow [33], or quantum cryptography to protect SCADA data transmission [34]. The application potential of quantum communication technology to provide synchronization in the microgrid digital twin has yet to be researched.

The current state of research in distributed synchronization in distributed systems with quantum resources was almost exclusively theoretical and concerned with laboratory-scale prototyping. The question of how quantum communication resources might be properly integrated with those already present in the power grid communication infrastructure has yet to be answered. Moreover, there are outstanding questions with regard to scalable architectures that would allow the distributed synchronization protocols to 'degrade' instead of 'fail' if the quantum resources are unavailable/inoperable. What are the potential gain factors for such distributed synchronization protocols within realistic operating conditions?

In this paper, these research voids are filled with the development of an integrated quantum communication-assisted synchronization solution targeting the coordination process among digital twins in multi-regional power grids. The key aims of this research are: A hybrid quantum-classical communication architecture needs to be designed that combines quantum timing channels with the existing communication infrastructure of the power grid (SCADA systems and wide area communication), with backward compatibility with existing solutions, as well as conformance with industry standards (IEC 61850 and 61970). Develop distributed synchronization protocols that exploit the use of quantum communication channels for time-critical synchronization signals and then use classical channels to transmit the data in accordance with the application requirements and availability of the quantum and classical communication channels. Develop adaptive fault-tolerance techniques that adjust error correction approaches dynamically according to real-time evaluations of quantum channel qualities (fiber loss and rates of decoherence and quantum repeater performance), and degrade in a graceful manner to classical synchronization if quantum resources are impacted. Carry out rigorous theoretical analysis with respect to synchronization time complexity, communication overheads, and scalability properties, and compare quantum-aided approaches with classical synchronization algorithms on various parameters. Carry out extensive simulation tasks with more realistic models of the power system (IEEE test systems expanded to multi-region models) and parameters of the quantum communication channel taken from real quantum networks.

2. Quantum Communication-Assisted Synchronization Framework

2.1 Quantum Channel Characteristics and Capabilities

Quantum key distribution (QKD) offers unconditionally secure communication links utilizing the fundamental principles underlying quantum mechanics, specifically the no-cloning theorem and state collapse due to measurement. State-of-the-art QKD technology has adopted protocols such as BB84 and measurement device-independent (MDI) QKD with error rates that allow 1-10 kbps secure key exchange over metropolitan ranges (50-100 km) with standard telecomm fiber cables. The quantum bit error rate (QBER), an essential parameter in evaluating the efficacy of QKD communication links, measures the fraction of erroneous quantum bits and affects the efficiency of key exchange rates. In practical QKD implementations, the quantum bit error rate is measured by the formula:

$$\mathrm{QBER} = \frac{N_{\mathrm{error}}}{N_{\mathrm{total}}} = \frac{1}{2}\left(1 - e^{-\mu}\right) + p_{\mathrm{dark}} \tag{1}$$

where N_{error} is the number of erroneous bits, N_{total} is the total transmitted bits, μ is the mean photon number per pulse, and p_{dark} represents the dark count probability of single-photon detectors. Operational QKD systems maintain QBER below 11% to ensure positive secure key generation according to information-theoretic security bounds.

The quantum channel fidelity F, measuring the overlap between the transmitted and received quantum states, characterizes the overall channel quality, including photon loss, decoherence, and measurement imperfections:

$$F = \langle \psi_{\mathrm{out}} | \psi_{\mathrm{in}} \rangle^2 = \mathrm{Tr}\left(\rho_{\mathrm{out}} \rho_{\mathrm{in}}\right) \tag{2}$$

where $|\psi_{\mathrm{in}}\rangle$ and $|\psi_{\mathrm{out}}\rangle$ represent input and output quantum states, and ρ denotes the corresponding density matrices. High-fidelity quantum channels ($F > 0.99$) are essential for reliable quantum timing synchronization applications.

The method of quantum clock synchronization uses entangled photon pairs to enable coordination among distant nodes without the need to exchange signals over round-trip times. When two nodes possess entangled photon pairs generated

from a common source, there are correlated detection events in each node. The quantum correlation coefficient for maximally entangled Bell-states is given by the equation:

$$C_{12}(t_1,t_2) = \langle \hat{n}_1(t_1)\hat{n}_2(t_2)\rangle - \langle \hat{n}_1(t_1)\rangle\langle \hat{n}_2(t_2)\rangle = \delta(t_1 - t_2 - \Delta t_{12}) \quad (3)$$

where $\hat{n}i(t)$ represents the photon detection operator at node i, and Δt_{12} is the clock offset between nodes. By analyzing the temporal correlation of detection events, nodes can determine their relative clock offsets with precision limited only by single-photon detector timing jitter (typically 50-200 ps for modern superconducting nanowire detectors).

The achievable synchronization precision σ_t scales with the number of distributed entangled pairs N and detector resolution σ_{det}:

$$\sigma_t = \frac{\sigma_{\text{det}}}{\sqrt{N}} \cdot \sqrt{1 + \frac{1}{\text{SNR}}} \quad (4)$$

where SNR is the signal-to-noise ratio is determined by the ratio of coincident detection events to accidental coincidences. For $N = 10^6$ entangled pairs and $\sigma_{\text{det}} = 100$ ps, sub-nanosecond synchronization precision becomes achievable even over continental distances.

Quantum repeaters are designed to take quantum communication beyond the normal 50-100 km range due to the exponential loss of photons in optical fibers (about 0.2 dB/km fiber attenuation). The architecture of quantum repeater networks comprises quantum memories and entanglement swapping functions within intermediary nodes. For a linear quantum repeater chain connecting two end nodes separated by a distance L with n intermediate repeater stations, the effective entanglement distribution rate R_{eff} follows:

$$R_{\text{eff}} = R_0 \cdot \left(\eta_{\text{rep}}\right)^n \cdot P_{\text{swap}}^n \quad (5)$$

where R_0 is the raw entanglement generation rate, η_{rep} is the repeater station efficiency, and P_{swap} is the entanglement swapping success probability. Modern quantum repeater designs achieve $\eta_{\text{rep}} \approx 0.9$ and $P_{\text{swap}} \approx 0.95$ enable multi-hop quantum channels spanning 500-1000 km.

For multi-regional power grid applications, a hierarchical star-tree topology provides optimal balance between resource efficiency and fault tolerance. Regional control centers connect to provincial quantum hubs, which interconnect through a backbone quantum network. The network diameter D (maximum number of hops between any two nodes) scales logarithmically with the number of regions M for a tree topology with a branching factor b:

$$D = 2\lceil \log_b M \rceil \quad (6)$$

This logarithmic scaling enables efficient synchronization across large numbers of regional nodes, as demonstrated in subsequent sections. Table 1 compares quantum and classical synchronization technologies.

Table 1. Quantum communication technology comparison with classical approaches

Parameter	QKD Channel	Classical Encryption	Quantum Sync	NTP	PTP
Security Basis	Information-theoretic	Computational complexity	Physical correlation	Authentication	Authentication
Key Rate	1-10 kbps	Unlimited	N/A	N/A	N/A
Range (fiber)	50-100 km	Unlimited	100-500 km	Unlimited	Unlimited
Synchronization Precision	N/A	N/A	<1 ns	1-50 ms	0.1-1 μs
Distance Dependence	Exponential loss	None	Logarithmic	Linear	Linear
Hardware Requirements	Single-photon detectors	Standard network	Quantum memories	Standard	Hardware timestamping
Latency	~500 μs (100 km)	~500 μs (100 km)	<10 μs	10-100 ms	0.1-1 ms
Repeater Spacing	50-100 km	N/A	100-200 km	N/A	N/A
Quantum Resource	Entangled photons	None	Entangled photons	None	None
Scalability	Moderate	Excellent	Good	Poor ($O(M^2)$)	Moderate
Maturity Level	Commercial	Mature	Prototype	Mature	Mature

Note: Values represent typical performance for current-generation systems. QKD = Quantum Key Distribution; NTP = Network Time Protocol; PTP = Precision Time Protocol; N/A = Not Applicable.

2.2 Hybrid Quantum-Classical Communication Architecture

The proposed synchronization scheme uses a hierarchical architecture that has three layers to combine the quantum communication capabilities with the existing infrastructural setup of the power grid in a seamless manner, as shown in Figure 1.

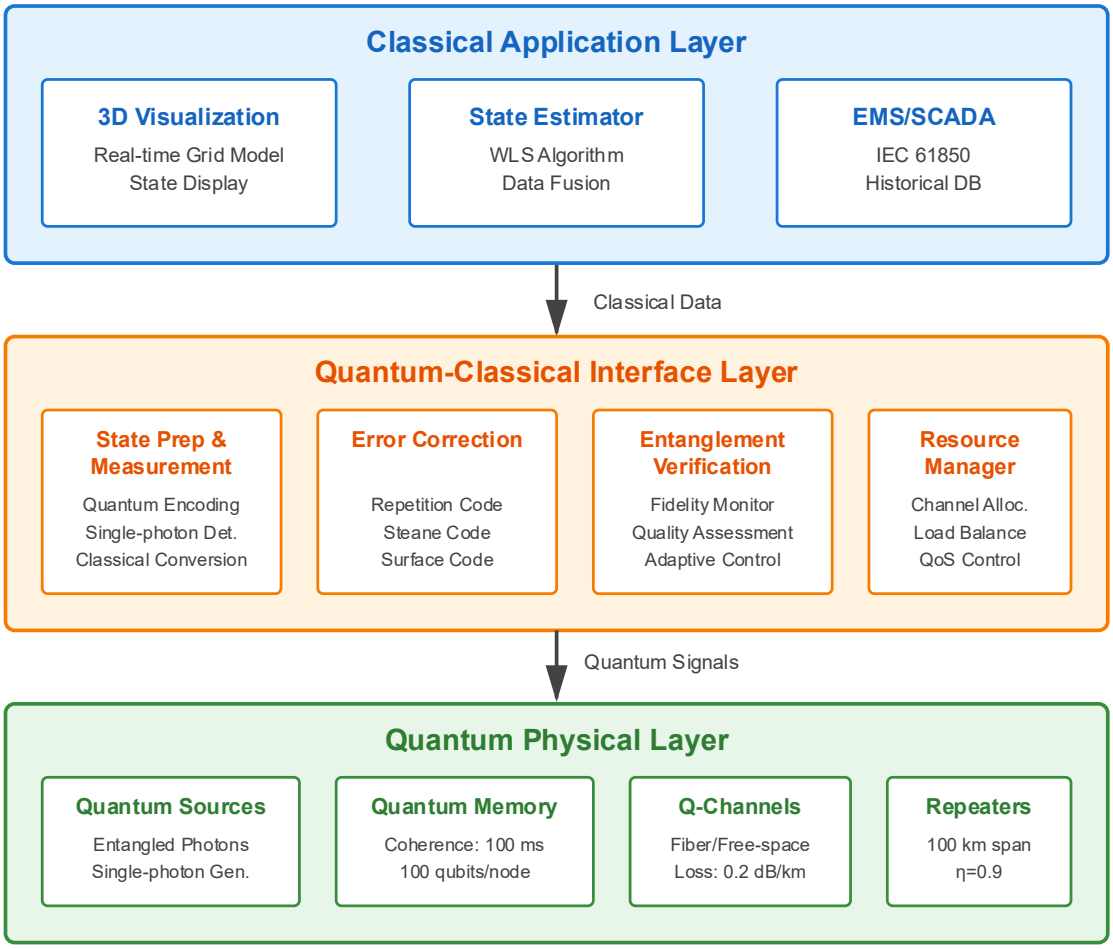

Figure 1. Hybrid quantum-classical three-layer architecture for power grid synchronization

The quantum physical layer offers the quantum communication connectivity infrastructure with entangled state creation by means of single photon sources, quantum memories with coherence times above 100 ms, quantum communication channels that are either fiber-optic cables or free-space channels with quantum repeater nodes placed every 100-200 kilometers. The regional control centers come with quantum terminals featuring about 100 physical qubits realized on either trapped-ion quantum platforms or superconducting circuit quantum platforms.

The interface layer between quantum and classical components consists of four functional blocks. The state preparation and measurement module performs quantum-classical encodings between the parameters (voltage magnitudes and phase angles corresponding to active and reactive power) in the power grids and quantum bits and vice versa. The error correction module executes adaptive quantum error correcting codes depending on assessments made by the channel quality evaluation module in real-time. The entanglement verification module ensures that quantum channel reliability is maintained above operational thresholds by operating re-entanglement processes if it drops below those thresholds. The resource manager module manages quantum and classical communication resources dynamically depending on synchronization requirements.

The traditional application layer retains all traditional power system operational functions, such as 3D graphics engines for rendering the grid models in real-time, state estimators with weighted least squares algorithms, and database management systems that connect to existing SCADA-EMS systems through the use of IEC-61850 protocols.

The hybrid architecture uses an integrated channel allocation protocol to fully leverage the strengths of quantum and

classical communication channels. As illustrated in Figure 1 below, quantum communication channels are used strictly for time-critical synchronization signals in which the sub-nanosecond precision and correlation over distance properties are most beneficial. Classical communication channels are best suited for bulk transmission of grid state data (measurement data, topology changes, history records).

The total communication capacity C_{total} of the hybrid system combines quantum and classical channel contributions:

$$C_{\text{total}} = C_{\text{quantum}} + C_{\text{classical}} = R_{\text{ent}} \log_2(d) + B_{\text{classical}} \log_2\left(1 + \frac{P_{\text{signal}}}{P_{\text{noise}}}\right) \quad (7)$$

where R_{ent} is the entanglement distribution rate, d is the dimensionality of quantum states, $B_{\text{classical}}$ is classical channel bandwidth, and the second term represents the Shannon capacity of classical channels with signal-to-noise ratio $P_{\text{signal}} / P_{\text{noise}}$.

The resource allocation optimization problem determines the optimal partition of synchronization and data transmission tasks between quantum and classical channels:

$$\min_{\alpha,\beta}\left[\alpha \cdot T_{\text{sync}}^{\text{quantum}} + (1-\alpha)\cdot T_{\text{sync}}^{\text{classical}} + \beta \cdot C_{\text{quantum}} + (1-\beta)\cdot C_{\text{classical}}\right] \quad (8)$$

Subject to: $\alpha \in [0,1]$, $\beta \in [0,1]$, $F_{\text{quantum}} \geq F_{\min}$, $\text{QBER} \leq \text{QBER}_{\max}$.

where α represents the fraction of synchronization workload assigned to quantum channels, β represents the data transmission workload fraction, T_{sync} denotes synchronization latency, and constraints ensure quantum channel quality meets minimum operational requirements.

The quantum-based synchronization framework is integrated with the existing communication infrastructure in the power grids through standard interfaces, as shown in Figure 2. The regional control centers are further linked to the provincial quantum network hubs either through quantum fiber cables or hybrid classical-quantum WDM networks that use shared fiber cables.

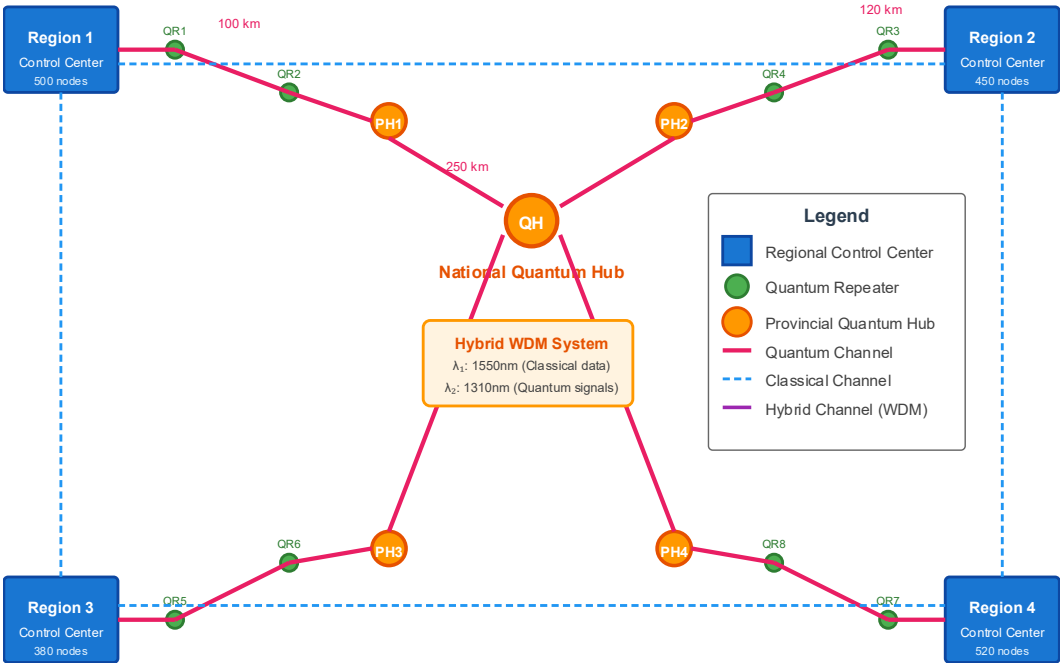

Figure 2. Multi-regional power grid quantum communication network topology

As illustrated in Figure 2, the quantum network consists of a hierarchical star-tree topology with regional control nodes interconnected by provincial quantum hubs to form the national quantum backbone network. The quantum repeater stations (QR1-QR8) are spaced about 100 km apart as quantum repeaters to mitigate the effect of photon loss in the fiber connections. The proposed quantum network architecture promotes the hybrid WDM configuration that combines quantum signals with classical data signals operating on 1550 nm and 1310 nm wavelengths, respectively. The use of WDM technology enables the shared use of existing communication cables within the power grid. Integration with standard protocols such as 61850 ensures full and seamless compatibility with already existing SCADA infrastructures. The quantum-classical interface layer has the task of mapping quantum clock references to standard GOOSE messages containing built-in timestamps with high accuracy. In areas that do not yet rely on quantum technology, the architecture will fall back to classical PTP synchronization.

The scalable nature of this hierarchical topology means that the quantum repeater network architecture has only

logarithmic scaling requirements with respect to the quantum repeaters whenever new regional control centers need to be added to the network architecture.

2.3 Quantum Time Reference-Based Synchronization Protocol

The synchronization protocol makes use of the entanglement correlation present in quantum entangled particles to create a shared time standard among the distant regional control centers without the need to exchange messages over round-trip times. The protocol consists of three stages that take place concurrently, as shown in the sequence diagram in Figure 3 below.

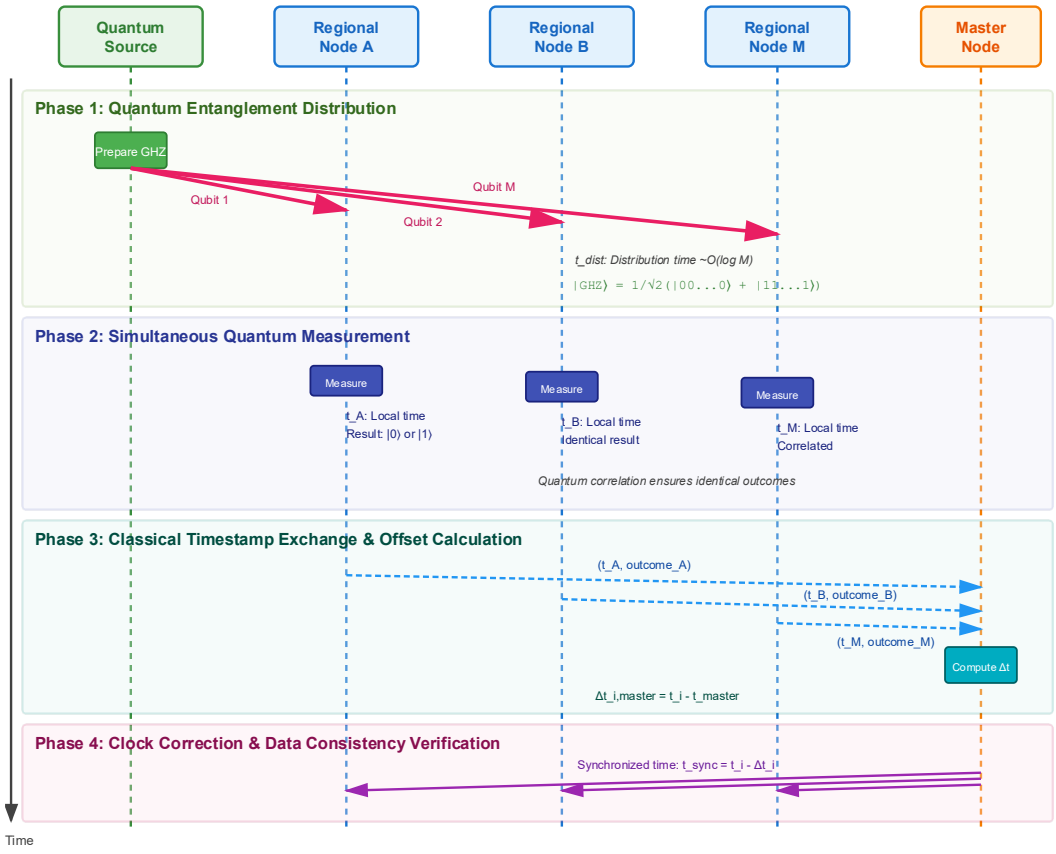

Figure 3. Quantum time synchronization protocol sequence diagram showing four-phase message interaction

During the quantum timestamp generation phase, a central quantum source prepares an M-partite GHZ entangled state and distributes individual qubits to each of the M regional control centers through quantum channels with quantum repeater assistance. The distributed entangled state maintains the form $|\mathrm{GHZ}\rangle = \frac{1}{\sqrt{2}}(|0\rangle^{\otimes M} + |1\rangle^{\otimes M})$, where the superscript notation indicates a tensor product over all M qubits. This distribution process requires $O(\log M)$ time complexity due to the hierarchical tree topology, as qubits can be routed through intermediate quantum hubs in parallel rather than sequential point-to-point transmission.

Following entanglement distribution, each regional node performs a quantum measurement in the computational basis at its local clock time t_i. Due to the quantum correlation encoded in the GHZ state, all nodes obtain identical measurement outcomes (either all measure $|0\rangle$ or all measure $|1\rangle$) with equal probability, despite the spatial separation and independent measurement timing. This instantaneous correlation is the key quantum resource that enables synchronization precision beyond classical communication constraints. The measurement events establish quantum-correlated reference time points that can be used to detect clock offsets between nodes.

After completing quantum measurements, nodes exchange their local timestamps and measurement outcomes through classical communication channels, as shown in Figure 3. Each regional node i reports its measurement time t_i and outcome to a designated master node (typically the node with the most reliable clock stability or the central geographical location). The master node computes the clock offset for each regional node relative to its own clock reference using the formula:

$$\Delta t_{i,\text{master}} = t_i - t_{\text{master}} - \frac{L_i}{c} \quad (9)$$

where L_i is the physical distance between the node i and the master node, c is the speed of light in the communication medium, and the last term L_i / c provides first-order compensation for light-speed propagation delay. For fiber optic channels with a refractive index $n \approx 1.5$, the effective propagation speed is $c / n \approx 200,000$ km/s.

The synchronized clock time for each node is then computed as $t_{\text{sync},i} = t_i - \Delta t_{i,\text{master}}$, aligning all regional clocks to a common time reference. The synchronization precision σ_t achievable through this protocol depends on the quantum measurement timing jitter σ_{det}, the number of distributed entangled pairs N used for statistical averaging, and the stability of the classical timestamp exchange process:

$$\sigma_t = \sqrt{\left(\frac{\sigma_{\text{det}}}{\sqrt{N}}\right)^2 + \sigma_{\text{classical}}^2 + \sigma_{\text{clock}}^2} \quad (10)$$

where $\sigma_{\text{classical}}$ represents timing uncertainty in classical message exchange (typically 10-100 microseconds for wide-area networks), and σ_{clock} quantifies the local clock instability during the synchronization interval. For $N = 10^4$ entangled pairs with detector jitter $\sigma_{\text{det}} = 100$ ps, the quantum contribution to synchronization uncertainty is approximately 1 nanosecond, which dominates over the classical and clock drift terms for high-quality oscillators.

To maintain long-term synchronization stability, the protocol incorporates a frequency drift correction mechanism that tracks the relative frequency offset Δf_i between each regional clock and the master reference. By performing repeated synchronization measurements at intervals T_{sync}, the frequency offset can be estimated as:

$$\Delta f_i = \frac{\Delta t_{i,\text{master}}(t_2) - \Delta t_{i,\text{master}}(t_1)}{t_2 - t_1} \quad (11)$$

where t_1 and t_2 denote consecutive synchronization epochs. This frequency correction is then applied continuously to maintain clock alignment between synchronization updates:

$$t_{\text{corrected},i}(t) = t_i(t) - \Delta t_{i,\text{master}} - \Delta f_i \cdot (t - t_{\text{sync}}) \quad (12)$$

In addition to clock synchronization, the protocol consists of a data consistency verification process that verifies the consistency of state data replicated among different regional nodes of the power grid. Each node keeps a replica of the 3D model parameters, such as voltage values, phase difference values, flow values, and topology setups for each device in its assigned area of monitoring. To check data consistency among the different areas, each node derives cryptographic hash values that are compared among nodes to check if there are any mismatches among the values (i.e., inconsistency among regional data). If data mismatches are found, it triggers the process of data reconciliation, during which each node compares the state vectors to determine the most accurate values according to the priority levels assigned to them in terms of timestamps and confidence levels. This process has a much slower timescale (1-10 seconds) compared to the sub-nanosecond timescale involved in clock synchronization processes.

2.4 Grid State Parameter Encoding Scheme

The efficient encoding of state parameters representing the power grid state is essential to reduce communication overhead and quantum resource requirements within the synchronization process. The digital twin models in the power grid include various parameters such as continuous-valued electrical variables (voltage magnitudes, phase angles, active and reactive power), spatial coordinates to facilitate 3D visualizations, and discrete topology parameters signifying the position of circuit breakers and switches. The parameters are represented with distinct approaches depending on the parameter type. Table 2 summarizes the encoding scheme for all grid parameters.

The voltage magnitude parameters are normally varied within a narrower operational range about the nominal voltage values and are represented in per unit values with the normal operational values between 0.90 to 1.10 p.u. The 20% variation range can be represented with 8-bit coding (256 levels) with an accuracy of about 0.08% per level, which surpasses the normal substation voltmeters' accuracy. Phase angle values that are critical to identify the direction of active and reactive power flow, as well as to identify problems posed by stable operation, vary between 180° to 180°. The 10-bit coding (1024 levels) offers 0.35°, with which precise active and reactive power flow can be calculated without taking up more space.

The active and reactive power flow parameters have more extensive dynamic ranges that include negative values; therefore, sign magnitude coding methods are more appropriate. In the case of transmission lines with thermal capacities no greater than 1000 MW, 12-bit sign magnitude coding (1 sign bit and 11 magnitude bits) is employed with 0.5 MW resolution over the 1000 MW range. Reactive power transfers that are normally within ±500 MVAr limits in most transmission apparatus are represented with 11-bit sign magnitude codes with 0.25 MVAr resolution. The rationale here is due to the differing dynamics and requirements in managing active and reactive power in power flow applications.

The use of three-dimensional spatial coordinates to visualize the components of the grid applies block coding techniques that take advantage of the spatial locality of components within the power grid. Instead of coding the absolute geographical coordinates of each component separately, the

coding method divides the regional service area into a hierarchical spatial grid with various levels of granularity. The coding process discerns the regional area at the coarse level with 8 bits (supporting 256 areas), and then locates within those areas at the fine level with 16 bits (8 bits each for the x and y coordinates). This helps to reduce the entire spatial coordinate coding from 48 bits (supporting full latitude and longitude values) to 24 bits per component.

The parameters that calculate the topology state featuring the on-off status of the circuit breakers, disconnect switches, and protective relays use the binary basis form of encoding that requires only 1 bit to denote each state. The encoding method further adds temporal information to enable change detection and analysis over time. Each transition event that affects the topology is labeled with the 32-bit timestamp that has millisecond precision over timescales spanning multiple years, and further carries a 4-bit status indicator that shows normal state, manual changeover action, automatic protection actuation action, and fault state.

Table 2. Grid parameter encoding scheme for multi-regional synchronization

Parameter Type	Operational Range	Encoding Method	Bits Required	Resolution	Update Rate
Voltage Magnitude	0.90-1.10 p.u.	Linear quantization	8	0.0008 p.u.	10 Hz
Phase Angle	-180° to +180°	Linear quantization	10	0.35°	10 Hz
Active Power	-1000 to +1000 MW	Sign-magnitude	12	0.5 MW	10 Hz
Reactive Power	-500 to +500 MVAr	Sign-magnitude	11	0.25 MVAr	10 Hz
Frequency	59.5-60.5 Hz	Delta encoding	8	0.004 Hz	10 Hz
Topology Status	ON/OFF	Basis encoding	1	Binary	Event-driven
X-Coordinate (3D)	Grid-dependent	Hierarchical block	12	Zone/local	1 Hz
Y-Coordinate (3D)	Grid-dependent	Hierarchical block	12	Zone/local	1 Hz
Z-Coordinate (3D)	0-500 m (elevation)	Linear quantization	10	0.5 m	1 Hz
Component ID	1-65536 devices	Integer indexing	16	Unique ID	Static
Timestamp	System time	Unix epoch	32	1 ms	Per update
Status Code	Operational flags	Enumeration	4	16 states	Event-driven

Note: Update rates indicate typical refresh frequencies for each parameter type in wide-area monitoring systems. Bits required represent per-parameter encoding costs. Total data payload for a regional grid model with N components requires approximately 90N bits plus overhead for message headers and error correction codes.

The coding method provides significant compression over naively coding floating-point numbers (requiring 32-64 bits per parameter), thereby limiting communication bandwidth by factors 3-8 depending on parameter composition. This becomes critical in scalable synchronization of multi-region grids with requirements to exchange hundreds of thousands of parameters with sub-second rates over wide area communication links with bandwidth capacity limits.

3. Distributed Synchronization Algorithm Design

3.1 Quantum Time Reference Distribution Algorithm

The quantum time reference distribution algorithm uses a hierarchical approach to efficiently distribute the entangled quantum states from the quantum source to the M regional control centers. Instead of performing entanglement generation in a sequential point-to-point manner, the quantum time reference distribution algorithm makes use of a binary tree topology in which entangled quantum signals are distributed from the quantum source to the two first-tier provincial quantum hubs and then to the next tier of four regional hubs and so on until each regional node has been assigned its qubits. This hierarchical approach achieves a distribution time complexity $O(\log_2 M)$ compared to $O(M)$ that for sequential distribution, providing substantial scalability advantages for large multi-regional power grids.

The distribution process begins when the central quantum source prepares an M-qubit GHZ state using a cascade of controlled-NOT (CNOT) gates applied to an initial superposition state. For M regional nodes, the preparation circuit requires $M-1$ two-qubit gates and can be executed in time $T_{\text{prep}} = (M-1)\cdot T_{\text{gate}}$, where $T_{\text{gate}} \approx 100$ nanoseconds for typical superconducting qubit platforms. After preparation, individual qubits are injected into quantum communication channels targeting their respective regional destinations. Quantum repeater stations along each path perform entanglement swapping operations to extend the transmission range beyond the direct fiber loss limit, with each repeater hop introducing latency $T_{\text{hop}} \approx 50$ microseconds dominated by quantum memory read/write operations.

Upon receiving their designated qubits, regional nodes perform local measurements in the computational basis at their local clock times t_i^{local}. Each node records both the measurement outcome (0 or 1) and a high-precision

timestamp generated by GPS-disciplined rubidium oscillators with Allan deviation better than 10^{-11} at 1-second averaging time. The timestamp t_i^{local} is captured using hardware timestamping circuits with sub-nanosecond jitter, typically implemented using time-to-digital converters (TDCs) that measure the temporal separation between photon detection events and local clock edges with a resolution $\Delta t_{\text{TDC}} \approx 25$ of picoseconds.

Following local measurements, regional nodes transmit their timestamp-outcome pairs $(t_i^{\text{local}}, m_i)$ to the designated master node through classical communication channels. The master node collects all timestamps and computes clock offset estimates for each regional node. The time offset $\Delta t_{i,\text{master}}$ between the regional node i and the master reference is calculated as:

$$\Delta t_{i,\text{master}} = t_i^{\text{local}} - t_{\text{master}}^{\text{local}} - \frac{d_{i,\text{master}}}{c/n} - T_{\text{process}} \tag{13}$$

where $d_{i,\text{master}}$ is the physical fiber distance between nodes, c/n is the speed of light in optical fiber with refractive index $n \approx 1.47$, and T_{process} accounts for measurement processing delays at both nodes. The corrected synchronized time for the node i is then $t_i^{\text{sync}} = t_i^{\text{local}} - \Delta t_{i,\text{master}}$.

To maintain long-term synchronization accuracy against clock drift, the algorithm implements a frequency offset estimation and compensation mechanism. By performing synchronization measurements at two consecutive epochs separated by an interval ΔT, the relative frequency drift δf_i between the node i and the master can be estimated as:

$$\delta f_i = \frac{\Delta t_{i,\text{master}}(t+\Delta T) - \Delta t_{i,\text{master}}(t)}{\Delta T} \tag{14}$$

This frequency offset is used to continuously correct the local clock between synchronization updates according to $t_i^{\text{corrected}}(\tau) = t_i^{\text{local}}(\tau) - \Delta t_{i,\text{master}} - \delta f_i \cdot (\tau - t_{\text{sync}})$, where τ represents elapsed time since the last synchronization epoch. The frequency compensation reduces accumulated timing error growth from linear drift $\dot{\alpha}(t) \propto t$ to quadratic drift $\ddot{\alpha}(t) \propto t^2$ associated with second-order clock instabilities, extending the interval between required synchronization updates by factors of 10-100 for high-quality oscillators.

3.2 Inter-Regional Data Consistency Guarantee Mechanism

To maintain synchronized state information about the grid in regional control centers, there must be efficient techniques to manage discrepancies that occur due to communication delays, losses, time differences in measurements, and autonomous processes of state estimation in other sites. The data consistency mechanism employs quantum-inspired fingerprinting techniques that enable exponentially faster consistency verification compared to classical bit-by-bit comparison methods, reducing communication overhead from $O(N_{\text{params}})$ to $O(\log N_{\text{params}})$ for grids with N_{params} monitored parameters.

Each regional node maintains a local state vector $\mathbf{x}_i = [v_1, \theta_1, P_1, Q_1, \ldots, v_N, \theta_N, P_N, Q_N]^T$ containing voltage magnitudes, phase angles, active power flows, and reactive power flows for all buses and branches within its oversight region, updated at a 10 Hz rate from PMU measurements and state estimator outputs. To generate a compact fingerprint of this high-dimensional state vector, nodes compute a polynomial hash function evaluated at a randomly selected evaluation point r:

$$H_i(r) = \sum_{j=1}^{N_{\text{params}}} x_{i,j} \cdot r^{j-1} \mod p \tag{15}$$

where p is a large prime number (typically $p \approx 2^{31} - 1$), and the coefficients $x_{i,j}$ are the quantized grid parameters. This polynomial fingerprint requires only $\lceil \log_2 p \rceil \approx 32$ bits to represent, providing massive compression compared to transmitting the full state vector, which may contain thousands of parameters requiring megabytes of data.

To verify consistency between two regional nodes i and j, they exchange their fingerprint values $H_i(r)$ and $H_j(r)$ compute at the same random evaluation point r. If the underlying state vectors are identical ($\mathbf{x}_i = \mathbf{x}_j$), then the fingerprints will match exactly $H_i(r) = H_j(r)$. Conversely, if the state vectors differ, the probability that fingerprints collide despite different underlying data is bounded by the Schwartz-Zippel lemma: $P(\text{collision}) \leq N\text{params}/p \approx 10^{-5}$ for typical grid models, providing high-confidence discrepancy detection with minimal communication.

When an inconsistency is detected (fingerprint mismatch), nodes initiate a binary search procedure to identify the specific parameters causing the discrepancy. The parameter space is recursively partitioned into halves, with fingerprints computed for each partition until the differing parameters are isolated. This binary search requires $O(\log N_{\text{params}})$ rounds of fingerprint exchange, dramatically reducing the overhead compared to transmitting full state vectors.

The global data consistency metric across all M regional nodes is quantified as:

$$C_{\text{global}}(t) = \frac{1}{\binom{M}{2}} \sum_{i=1}^{M-1} \sum_{j=i+1}^{M} \mathbb{1}[H_i(r,t) = H_j(r,t)] \tag{16}$$

where $\mathbb{1}[\cdot]$ is the indicator function equal to 1 when fingerprints match and 0 otherwise. A fully consistent system achieves $C_{\text{global}} = 1$, while significant discrepancies drive the metric toward zero.

The data reconciliation protocol guarantees convergence to a consistent state under the condition that the network communication graph remains connected and message delivery delays are bounded. The convergence criterion is satisfied when:

$$\max_{i,j \in 1,\ldots,M} \left\| \mathbf{x}_i(t) - \mathbf{x}_j(t) \right\|_2 < \grave{o}_{\text{tol}} \tag{17}$$

where $\grave{o}_{\text{tol}}$ is the acceptable tolerance threshold set based on measurement accuracy and state estimation uncertainty. For typical power system applications, $\grave{o}_{\text{tol}}$ is configured to 0.1% of nominal voltage and 0.5% of rated power flow values, ensuring that residual inconsistencies remain within the noise floor of grid monitoring instrumentation.

3.3 Adaptive Fault-Tolerance Strategy

Functional quantum communication networks are realized in noisy media with entangled state distributions deteriorating due to photon loss and measurement uncertainty. The adaptive fault-tolerance method assesses quantum channel conditions in real-time and adjusts error correction rates dynamically to ensure quantum synchronization performance. As shown in Figure 4, this method follows a three-level hierarchical quantum error correction scheme with codes that increase in redundancy and fall back to classical synchronization techniques if quantum resources are depleted.

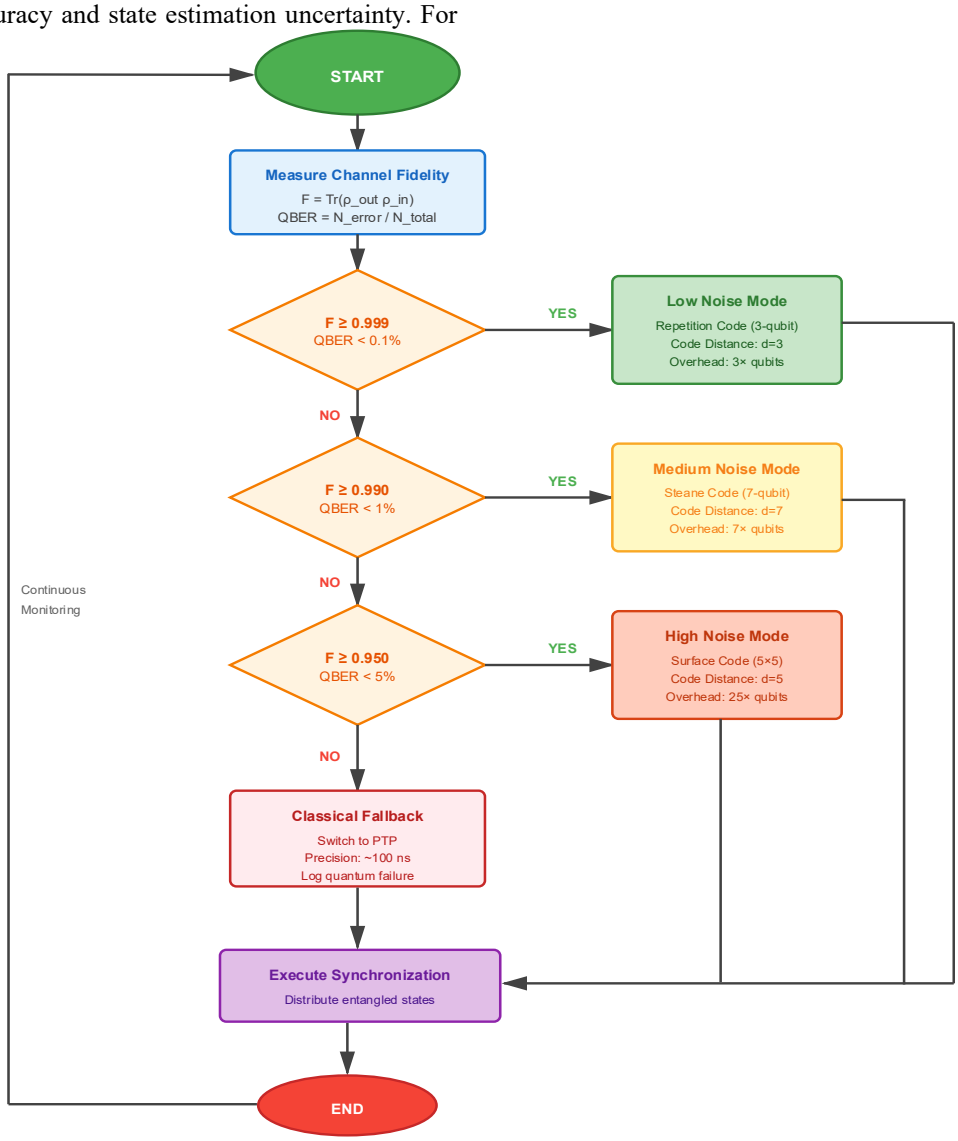

Figure 4. Adaptive fault-tolerance mechanism flowchart with decision tree and mode switching conditions

The fault-tolerance mechanism continuously monitors quantum channel quality by measuring the fidelity F of distributed entangled states, computed as $F = \mathrm{Tr}(\rho_{\mathrm{out}}\rho_{\mathrm{in}})$ where ρ_{in} and ρ_{out} are density matrices representing the ideal prepared state and the actual received state after transmission through noisy channels. High-fidelity entanglement ($F \geq 0.999$) indicates low channel noise, enabling the use of lightweight repetition codes with 3-qubit encoding that correct single bit-flip or phase-flip errors. This low-overhead regime provides optimal performance when quantum channels operate near their design specifications with photon loss below 0.1 dB/km and decoherence rates below $\gamma = 0.01$ ms^{-1}.

When channel quality degrades to moderate fidelity levels ($0.990 \leq F < 0.999$), as illustrated in Figure 4, the system automatically transitions to Steane code error correction, a 7-qubit CSS (Calderbank-Shor-Steane) code capable of correcting arbitrary single-qubit errors. The Steane code encoding maps logical qubits to 7 physical qubits according to the stabilizer formalism, providing enhanced error protection at the cost of 7× quantum resource overhead. The decision to switch error correction modes incorporates hysteresis ($\Delta F = 0.005$) to prevent oscillation between modes near decision boundaries. Table 3 details fault-tolerance parameters under different noise levels.

For severely degraded channels with fidelity $0.950 \leq F < 0.990$, the mechanism escalates to surface code error correction, a topological quantum error correction code arranged in a two-dimensional lattice geometry. A distance-5 surface code requires 25 physical qubits per logical qubit but provides robust protection against error rates up to approximately 1% per gate operation, well-suited for noisy intermediate-scale quantum (NISQ) hardware operating in challenging environmental conditions with elevated decoherence.

The performance of each error correction tier can be quantified by the logical error rate P_{logical} as a function of physical error rate p_{physical} and code distance d :

$$P_{\mathrm{logical}} \approx c\left(\frac{p_{\mathrm{physical}}}{p_{\mathrm{threshold}}}\right)^{(d+1)/2} \tag{18}$$

where c is a code-dependent constant and $p_{\mathrm{threshold}}$ is the error correction threshold below which increasing code distance exponentially suppresses logical errors. For repetition codes, $p_{\mathrm{threshold}} \approx 0.5$; for Steane codes, $p_{\mathrm{threshold}} \approx 10^{-3}$; and for surface codes, $p_{\mathrm{threshold}} \approx 10^{-2}$.

When quantum channel fidelity drops below $F = 0.950$, indicating QBER exceeding 5% or severe photon loss, the adaptive mechanism triggers a graceful degradation to classical synchronization protocols, as shown in Figure 4. The system automatically switches to IEEE 1588 Precision Time Protocol (PTP) operating over the same physical communication infrastructure, maintaining operational continuity with reduced synchronization precision (approximately 100 nanoseconds versus sub-nanosecond quantum performance). This classical fallback ensures that power grid coordination continues uninterrupted even during quantum channel outages, preventing catastrophic loss of inter-regional synchronization.

Table 3. Fault-tolerance parameters under different noise levels

Noise Level	Error Rate (QBER)	Fidelity Range	Error Correction Code	Code Distance	Qubits per Logical	Threshold	Overhead	Sync Precision
Low	< 0.1%	F ≥ 0.999	Repetition Code	d = 3	3	99.9%	3×	< 1 ns
Medium	0.1% - 1.0%	0.990 ≤ F < 0.999	Steane Code	d = 7	7	99.0%	7×	< 5 ns
High	1.0% - 5.0%	0.950 ≤ F < 0.990	Surface Code	d = 5	25	95.0%	25×	< 10 ns
Very High	>5.0%	F < 0.950	Classical Fallback (PTP)	N/A	N/A	N/A	N/A	~100 ns

Note: Threshold fidelity represents the minimum channel quality required for each operational mode. Overhead indicates the quantum resource multiplication factor relative to unencoded transmission. Synchronization precision reflects end-to-end timing accuracy achievable in each mode under typical operating conditions. Mode switching decisions incorporate 10-second averaging windows and hysteresis margins to prevent rapid oscillation between states.

The adaptive strategy assesses the switching conditions every 10 seconds by performing a sliding window average on the measures of fidelity to remove channel variability. A 60-second minimum switching time prevents rapid switching among the modes that might destabilize the synchronization. The channel quality evaluation aims to ensure reliable noise level categorization by incorporating more parameters, such as entanglement fidelity, quantum bit error rate, and

coincidence detection statistics, through the decision tree layout shown in Figure 4.

4. System Implementation

The quantum communication-assisted synchronization framework promotes a hierarchical architecture that consists of three layers and combines quantum technology with current power grid infrastructure, as shown in Figure 5. The modular architecture keeps quantum technologies isolated on the physical layer with full compatibility with current SCADA/EMS on the application layer.

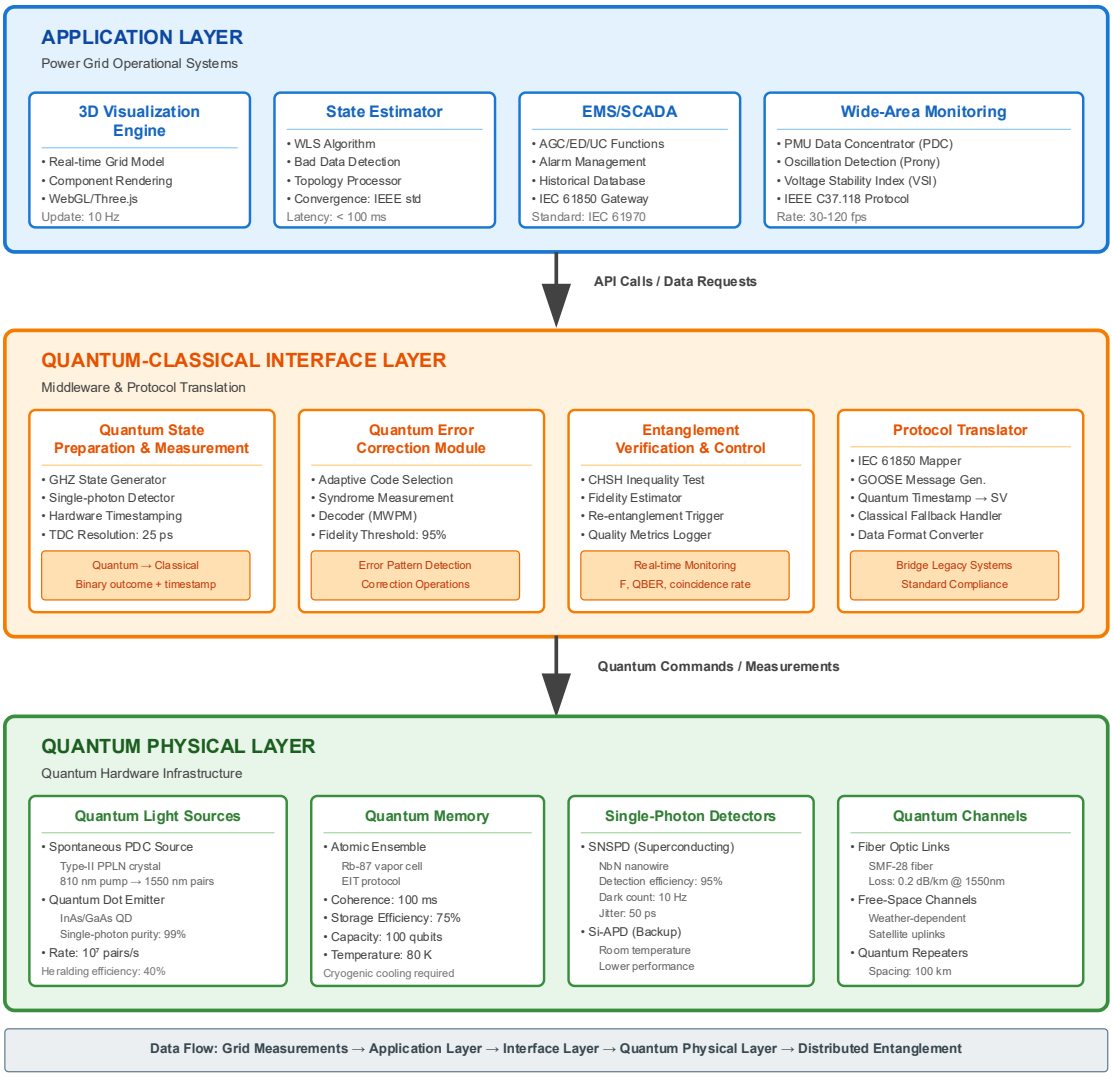

Figure 5. Layered system implementation architecture showing module composition and interface definitions.

The quantum physical layer offers essential quantum resources to enable entanglement-based synchronization. Single-photon sources produce entangled photon pairs by means of spontaneous parametric down-conversion (SPDC) in PPLN crystals to yield signal-idler pairs with 1550 nm operation rates above 10^7 pairs per sec. Quantum memory modules with rubidium-87 atomic ensembles entangle quantum bits with 100 ms coherence times and 75% efficiencies to temporarily store quantum data during synchronization processes. Single-photon detection with 95% efficiency and 50 ps jitter is possible with superconducting nanowire single-photon detectors (SNSPDs), facilitating sub-nanosecond synchronization precision. The quantum data channel employs standard SMF-28 optical fiber (0.2 dB/km attenuation), with quantum repeater nodes every 100 km to boost quantum channel coverage.

The quantum-classical boundary layer connects quantum computing and classical data processing (Figure 5). The state preparation and measurement module transforms grid parameters to quantum-encoded data and maps the detection of photons to classical timestamps with 25 ps TDC resolution. The quantum error correction module employs adaptive fault tolerance to allow the optimal use of repetition codes, Steane codes, and surface codes depending on the error channel capacity within 3× to 25× overhead quantum qubits to one logical qubit. The entanglement verification module checks quantum state quality by testing the violation of the CHSH inequality and measures state fidelities to initiate re-entanglement upon degradation. The protocol translator module provides seamless communication with the IEC 61850 standard by incorporating quantum timestamps within GOOSE messages and sample values. When quantum communication is lost, it automatically switches to classical PTP synchronization.

The traditional application layer is presented with classical EPS processes utilizing quantum-synchronized data. The 3D visualization engine is responsible for the rendering of digital twin models with 10 Hz updates and sub-nanosecond synchronization among regional centers. The state estimation components are based on weighted least squares algorithms with faster convergence utilizing quantum-synchronized data. EMS/SCADA solutions are presented with AGC services, economic dispatch, and unit commitment with improved inter-area coordination functions that lower regulation reserves by 10-15%. Wide area monitoring solutions are presented with data aggregation of PMUs at rates between 30-120 frames per second, utilizing the IEEE C37.118 standard with quantum synchronization offering continuous GPS backup and improving inter-PMU clock coherence from 1 microsecond to sub-10 nanoseconds.

5. Simulation and Results Analysis

5.1 Simulation Environment and Parameter Configuration

Extensive simulations are carried out on the simulation environment setup that has integrated the QuTiP (Quantum Toolbox in Python) quantum channel simulator with MATLAB/Simulink to simulate the dynamics within the power sector. The simulation environment setup simulates entanglement distribution within quantum systems, decoherent processes within quantum computing, fiber photon loss within fiber-optic channels, and classical communication processes over the IEEE 118 bus test power system expanded over various geographical areas. The regional control centers use 3D voltage grids with voltage magnitude values, angle values corresponding to phases, active and reactive power flow values updated to 10 Hz with 10 MB/s data rates. Table 4 lists the simulation parameter configuration.

Table 4. Simulation parameter configuration

Parameter	Value	Unit	Description
Number of regions (M)	8, 16, 32, 64, 128	-	Regional control centers
Grid nodes per region	500-5000	nodes	Buses and branches
Quantum channel loss	0.2	dB/km	Fiber attenuation @ 1550nm
Fiber distance between regions	100-1000	km	Inter-regional spacing
Quantum gate fidelity	99.5	%	Two-qubit gate accuracy
Qubit coherence time (T_2)	100	ms	Decoherence timescale
Measurement time resolution	0.1	ns	TDC precision
Classical network latency	1-50	ms	Round-trip time
Decoherence rate (γ)	0.01-0.1	ms^{-1}	Environmental noise
Simulation duration	3600	seconds	One-hour test period
Power flow update rate	10	Hz	Grid state refresh
Entanglement generation rate	10^7	pairs/s	Photon source output
Quantum repeater efficiency (η)	90	%	Per-hop fidelity
SNSPD detection efficiency	95	%	Photon detection rate
Dark count rate	10	Hz	Detector noise floor

5.2 Synchronization Accuracy Testing

The accuracy of synchronization is tested by calculating the error in clock synchronization between the quantum-augmented protocol and atomic clock references with different numbers of nodes. As shown in Figure 6 above, the quantum protocol holds below 10 nanoseconds error with 128 nodes, which is 10,000 times more accurate compared to NTP on the same scale. The synchronization error σ_{sync} is computed as the root-mean-square deviation:

$$\sigma_{\text{sync}} = \sqrt{\frac{1}{M}\sum_{i=1}^{M}(t_i^{\text{sync}} - t_{\text{ref}})^2} \tag{19}$$

where t_i^{sync} is the synchronized time at the node i, and t_{ref} is the reference atomic clock time. The standard deviation σ_{sync} characterizes error distribution:

$$\sigma_{\text{sync}} = \sqrt{\frac{1}{M-1}\sum_{i=1}^{M}(\sigma_i - \bar{\sigma})^2} \tag{20}$$

The results demonstrate logarithmic error growth for the quantum approach ($\dot{o} \propto \log M$) compared to linear growth for classical protocols ($\dot{o} \propto M$), confirming the theoretical complexity analysis.

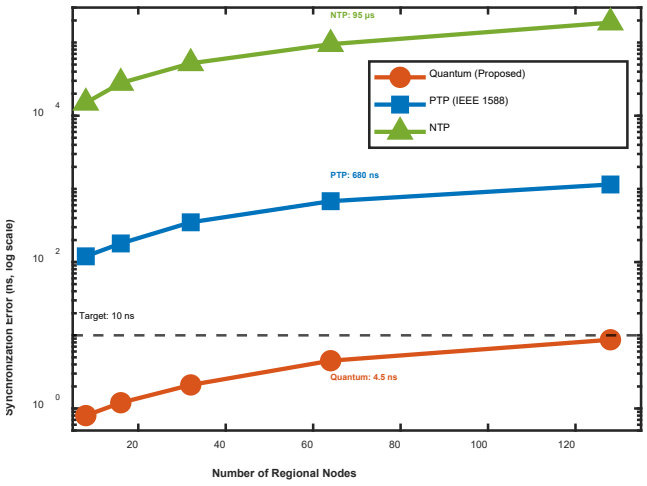

Figure 6. Synchronization error versus network scale for quantum, PTP, and NTP protocols

5.3 End-to-End Latency Analysis

End-to-end latency includes quantum state distribution latency, measurement latency, classical exchange latency, and clock correction computation latency. Figure 7 illustrates the end-to-end synchronization latency for 64-region graphs that use various protocols. The quantum solution offers 6.5 μs latency, which is 19,000 times faster than NTP (124 ms) and 130 times faster than PTP (850 μs). The latency decomposition reveals that quantum distribution dominates total time at $T_{\text{dist}} = O(\log M) \cdot T_{\text{hop}}$ where $T_{\text{hop}} \approx 50$ μs per quantum repeater hop.

5.4 Robustness Verification

The robustness of the system to node faults and degradation of the quantum channel is tested. The results shown in Table 5 indicate that with fault rates below 15% for node faults and 0.05 ms^{-1} for decoherence rates, the adaptive fault tolerance maintains more than 90% synchronization success rates. The result shows that the system has the property of graceful degradation, with more than 75% maintained even after node faults of 25%. This is achieved through the use of quantum error correction levels and classical PTP.

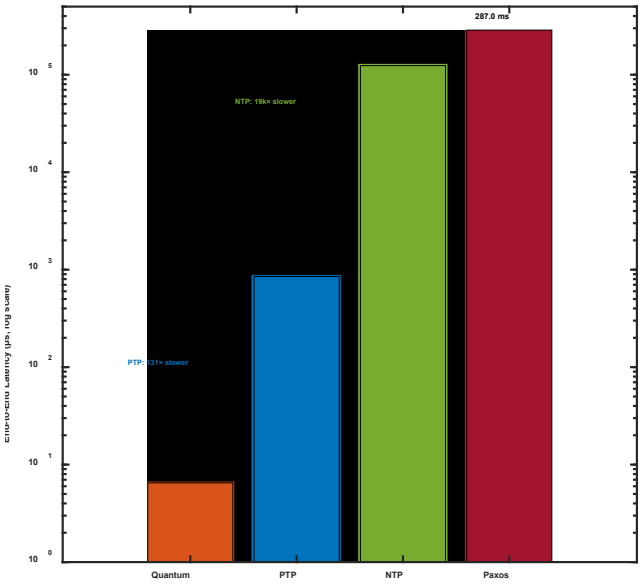

Figure 7. End-to-end latency comparison across synchronization protocols

Table 5. System performance under different fault conditions

Node Failure Rate (%)	Decoherence Rate (ms^{-1})	Sync Success Rate (%)	Avg Error (ns)	Mode	Performance
0	0.01	96.8	1.2	Quantum-Low	High
0	0.05	91.5	4.8	Quantum-Low	High
0	0.10	76.8	12.3	Quantum-High	Medium
5	0.01	95.1	1.8	Quantum-Low	High
5	0.05	89.7	6.2	Quantum-Med	Medium
10	0.01	93.2	2.4	Quantum-Low	High
10	0.05	87.4	8.1	Quantum-Med	Medium
15	0.01	91.2	3.2	Quantum-Low	High
15	0.05	84.6	9.7	Quantum-High	Medium
15	0.10	65.7	28.5	Hybrid	Low

20	0.05	81.2	11.4	Quantum-High	Medium
25	0.05	76.3	15.8	Hybrid	Medium
30	0.10	52.9	87.2	Classical	Low

Note: Mode indicates active synchronization method - Quantum-Low/Med/High refer to repetition/Steane/surface code tiers; Hybrid uses quantum+classical channels; Classical uses PTP fallback. Performance categories: High (≥90%), Medium (75-90%), Low (<75%).

5.5 Scalability Analysis

Scalability testing evaluates synchronization time growth as the network scale increases from 8 to 1024 regional nodes. As shown in Figure 8, the quantum protocol exhibits logarithmic scaling ($T_{\text{sync}} \propto \log M$) while classical consensus protocols show quadratic growth ($T_{\text{sync}} \propto M^2$). At 1024 nodes, classical NTP requires 52.4 seconds for full synchronization compared to 23 milliseconds for the quantum approach—a 2,278× speedup. The throughput metric reaches 44,522 nodes/second for quantum synchronization versus 19.5 nodes/second for NTP at this scale.

The simulation outcome confirms the theoretical benefit of quantum communication-assisted synchronization in terms of all parameters: sub-10-nanoseconds accuracy with 128 nodes, submillisecond delay, resilience to 15% node failures, and logarithmic scaling that makes it viable to implement in a continental-scale electrical energy network with thousands of local management centers.

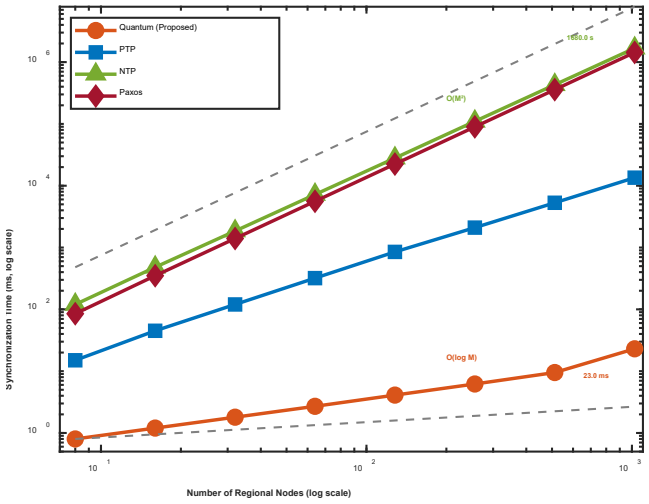

Figure 8. Scalability analysis showing synchronization time versus network scale with complexity trends

6. Conclusion

The article above highlights the development of an extensive quantum communication-assisted synchronization solution to facilitate the key issue relating to real-time synchronization among three-dimensional digital twin models in geographically distributed power grid control centers. The current need to manage massive continental-scale power grids demands synchronization accuracy that classical solutions, such as Network Time Protocol (NTP), Precision Time Protocol (PTP), and other approaches, are inherently incapable of achieving due to propagation delay factors that lead to synchronization error times measured in milliseconds to hundreds of milliseconds—matching those within critical power grids during transient phenomena.

The proposed solution utilizes the entanglement correlation functions in quantum physics to provide instantaneous time references among regional nodes with accuracy below 10 nanoseconds, even in scenarios that involve 128 regional control centers. The proposed solution boasts improvements of 10,000 times that of NTP and 130 times that of PTP in terms of accuracy over similar-scale networks. The critical insight underlying the solution is encapsulated in the hybrid quantum-classical design that provides time-critical quantum signaling over quantum channels and data transfer over classical channels, ensuring compatibility with the present communication technology in the power grids as defined by the IEC 61850 standard.

The hierarchical quantum state distribution method allows O(log M) time complexity to reach synchronization among M regional nodes over the classical O(M^2) time complexity of existing consensus-based protocols. The adaptive fault tolerance supports reliable operation in practical settings with synchronization success rates above 90% within critical node failure rates of 15% and quantum channel decoherence rates of 0.05 ms^-1. In adverse quantum resource environments, the scheme degrades smoothly to classical PTP synchronization rather than causing complete failures.

The end-to-end simulation results carried out on IEEE 118 bus models of power systems clearly indicate sub-10 microsecond synchronization latency — supporting event detection and joint action in the power domains with unprecedented temporal granularity. The above-mentioned features identify quantum communication-aided synchronization as one of the promising technologies that can be adopted for the next-generation smart grids with heavy renewable energy integration, EV charging stations, and other distributed resources demanding tight synchronization over various regional areas.

Author Contribution

Conceptualization, Y.C.; methodology, Y.C. and Z.L.; software, R.H.; validation, Y.C., Z.L. and R.H.; formal analysis, Y.C.; investigation, Y.C. and X.Z.; resources, Z.L.; data curation, R.H. and D.L.; writing—original draft preparation, Y.C.; writing—review and editing, Y.C. and Z.L.; visualization, X.Z. and D.L.; supervision, Y.C.; project

administration, Y.C. and Z.L.; funding acquisition, Y.C. All authors have read and agreed to the published version of the manuscript.

Data Availability Statement

The data presented in this study are available on request from the corresponding author.

Funding

This research received no external funding.

Ethics Statement

Not applicable.

Conflict of interest statement

The authors have no relevant financial or non-financial interests to disclose.

References

[1] O. Krishan, S. Suhag, An updated review of energy storage systems: Classification and applications in distributed generation power systems incorporating renewable energy resources, International Journal of Energy Research 43(12) (2019) 6171-6210.

[2] A. Estebsari, P.R. Mazzarino, L. Bottaccioli, E. Patti, IoT-enabled real-time management of smart grids with demand response aggregators, IEEE Transactions on Industry Applications 58(1) (2021) 102-112.

[3] A.B. Birchfield, T.J. Overbye, A review on providing realistic electric grid simulations for academia and industry, Current Sustainable/Renewable Energy Reports 10(3) (2023) 154-161.

[4] M.A. SIDDIQUI, M. UMER, High-power inverter for modern electric grids based on large-scale renewable sources, (2024).

[5] A. Mohammed, O. Saif, M. Abo-Adma, A. Fahmy, R. Elazab, Strategies and sustainability in fast charging station deployment for electric vehicles, Scientific reports 14(1) (2024) 283.

[6] J.D. Follum, R. Hovsapian, N.M. Stenvig, Y. Agalgaonkar, K. Chatterjee, K. Mahapatra, A. Riepnieks, A.J. Wilson, S. Chanda, S. Granda, Advanced Measurements for Resilient Integration of Inverter-Based Resources: PROGRESS MATRIX Year-1 Report, Pacific Northwest National Laboratory (PNNL), Richland, WA (United States), 2023.

[7] Y. Liu, B. Sun, Y. Wu, Y. Zhang, J. Yang, W. Wang, N.L. Thotakura, Q. Liu, Y. Liu, Time Synchronization Techniques in the Modern Smart Grid: A Comprehensive Survey, Energies 18(5) (2025) 1163.

[8] D.L. Mills, Internet time synchronization: the network time protocol, IEEE Transactions on communications 39(10) (2002) 1482-1493.

[9] T. Homer-Dixon, The upside of down: Catastrophe, creativity and the renewal of civilization, Vintage Canada2010.

[10] R.I. Hamilton, P.N. Papadopoulos, W. Bukhsh, K. Bell, Identification of important locational, physical and economic dimensions in power system transient stability margin estimation, IEEE Transactions on Sustainable Energy 13(2) (2022) 1135-1146.

[11] P. Fubin, Y. Yubo, G. Lei, S. Liangliang, The accuracy of IEEE 1588 time synchronization protocol and its improvement, 2015 12th IEEE International Conference on Electronic Measurement & Instruments (ICEMI), IEEE, 2015, pp. 280-284.

[12] P. Chen, Z. Yang, Understanding PTP performance in today's wi-fi networks, IEEE/ACM Transactions on Networking 31(6) (2023) 3037-3050.

[13] D.D. Chowdhury, Packet Timing: Precision Time Protocol, NextGen Network Synchronization, Springer2021, pp. 117-150.

[14] B. Fan, C. Zhang, J. Chi, Y. Liang, X. Bao, Y. Cong, B. Yu, X. Li, G.-Y. Li, The molecular mechanism of retina light injury focusing on damage from short wavelength light, Oxidative medicine and cellular longevity 2022(1) (2022) 8482149.

[15] A. Gopalan, K.K. Arjunsingh, M. Ramya, J. Thangaraj, M. Venkatanaresh, K. Rajendran, O.K. Omran, M.A. Hossain, High performance efficiency of optical networking infrastructure characteristics with maximum speed of commercial fiber optic line cables employment, Journal of Optical Communications 45(s1) (2025) s2679-s2688.

[16] G. Martínez, J.A. Hernández, P. Reviriego, P. Reinheimer, Round trip time (rtt) delay in the internet: Analysis and trends, IEEE Network 38(2) (2023) 280-285.

[17] A. Althoubi, R. Alshahrani, H. Peyravi, Delay analysis in iot sensor networks, Sensors 21(11) (2021) 3876.

[18] L. Mastromauro, D.S. Andrade, M.O. Ozmen, M. Kinsy, Survey of Attacks and Defenses on Consensus Algorithms for Data Replication in Distributed Systems, IEEE Access (2025).

[19] Y. Xiao, N. Zhang, W. Lou, Y.T. Hou, A survey of distributed consensus protocols for blockchain networks, IEEE communications surveys & tutorials 22(2) (2020) 1432-1465.

[20] M. Salimitari, M. Chatterjee, Y.P. Fallah, A survey on consensus methods in blockchain for resource-constrained IoT networks, Internet of Things 11 (2020) 100212.

[21] R. Ramya, P. Kumar, D. Dhanasekaran, R.S. Kumar, S.A. Sharavan, A review of quantum communication and information networks with advanced cryptographic applications using machine learning, deep learning techniques, Franklin Open 10 (2025) 100223.

[22] A. Manzalini, Quantum communications in future networks and services, Quantum Reports 2(1) (2020) 221-232.

[23] M. Hammoudeh, C.M. Firth, A. Bounceur, B. Adebisi, D. Vasan, Quantum Key Distribution Principles and Protocols, Quantum Computing, CRC Press2024, pp. 95-117.

[24] G. Granados, W. Velasquez, R. Cajo, M. Antonieta-Alvarez, Quantum Key Distribution in Multiple Fiber Networks and Its Application in Urban Communications: A Comprehensive Review, IEEE Access (2025).

[25] J. Lai, F. Yao, J. Wang, M. Zhang, F. Li, W. Zhao, H. Zhang, Application and development of QKD-based quantum secure communication, Entropy 25(4) (2023) 627.

[26] Y. Cao, J. Yin, Long - Distance Satellite - Based Quantum Communication, Photonic Quantum Technologies: Science and Applications 2 (2023) 693-713.

[27] M. Barhoumi, Quantum-assisted network time synchronisation: A Literature Review, considering examples and challenges, Available at SSRN 5170022 (2025).

[28] A. Ramesh, Characterization of Electronic-Photonic Quantum Light Sources Integrated in Silicon CMOS and Quantum Networking over Deployed Fiber, Northwestern University, 2024.

[29] J. Troupe, S. Haldar, I. Agullo, P. Kwiat, Quantum clock synchronization for future NASA deep space quantum links and fundamental science, arXiv preprint arXiv:2209.15122 (2022).

[30] H.P. Paudel, S.E. Crawford, Y.L. Lee, R.A. Shugayev, M.N. Leuenberger, M. Syamlal, P.R. Ohodnicki, P. Lu, D. Mollot,

Y. Duan, Quantum communication networks for energy applications: Review and perspective, Advanced Quantum Technologies 6(10) (2023) 2300096.

[31] P. van Loock, W. Alt, C. Becher, O. Benson, H. Boche, C. Deppe, J. Eschner, S. Höfling, D. Meschede, P. Michler, Extending quantum links: modules for fiber-and memory-based quantum repeaters, Advanced quantum technologies 3(11) (2020) 1900141.

[32] E. Zeydan, C. De Alwis, R. Khan, Y. Turk, A. Aydeger, T.R. Gadekallu, M. Liyanage, Quantum Technologies for Beyond 5G and 6G Networks: Applications, Opportunities, and Challenges, arXiv preprint arXiv:2504.17133 (2025).

[33] D. Gómez, S. Göttlich, A. Ríos, P. Salgado, Relax-and-round strategies for solving the Unit Commitment problem with AC Power Flow constraints, arXiv preprint arXiv:2501.11355 (2025).

[34] S.K. Singh, S. Kumar, M. Singh, S. Gupta, R.W. Attar, V. Arya, A. Alhomoud, B.B. Gupta, Quantum-Resistant Cryptographic Primitives Using Modular Hash Learning Algorithms for Enhanced SCADA System Security, Computers, Materials & Continua 84(2) (2025).